

## FROM PIXELS TO VOXELS: TRACKING VOLUME ELEMENTS IN SEQUENCES OF 3-D DIGITAL IMAGES

Hans-Gerd Maas, Anthony Stefanidis, Armin Gruen

Institute of Geodesy and Photogrammetry, Swiss Federal Institute of Technology  
ETH-Hoenggerberg, CH - 8093 Zurich, Switzerland  
Tel. +41-1-6333058, Fax +41-1-6331101, e-mail: gerd or tony or agruen @p.igp.ethz.ch

ISPRS Commission III, Intercommission Working Group V/III

**KEY WORDS:** tomography data, least squares matching, tracking, voxels

### ABSTRACT

This paper presents the extension of certain, fundamental digital photogrammetric concepts, theories and strategies to three dimensions, and their performance in an interdisciplinary application for 3-D image sequence analysis in a technical chemistry experiment. Specifically, we present an image analysis technique for examining the fine scale (Kolmogorov scale) variations of the mixing process in a turbulent flow. The objective is to trace the interaction of two flows by identifying their motions in a sequence of 3-D images obtained with a system based on a high-speed solid state camera. After briefly describing the imaging process and the particularities related to the capture of quasi-continuous 3-D image sequences, we focus on theoretical and implementational issues associated with feature tracking in 3-D image sequences. We present the extension of least squares matching from pixels, associated with 2-D images, to voxels, associated with 3-D images. The use of additional constraints of radiometric and/or geometric nature strengthens the matching solution. In addition, the large amount of data associated with 3-D image sequences in general, and the high and multidirectional velocities involved in this application in particular, make the devising of an efficient matching strategy quite important.

### 1. INTRODUCTION

The methods used for the measurement of velocity fields in flows can be distinguished into *single-point* techniques, aiming at the determination of the velocity vector (or components of it) at one point with high temporal resolution, and *multi-point* techniques, aiming at the simultaneous determination of multiple velocity fields. The latter are usually based on flow visualization, which can either be attained in *discrete* manner by seeding with particles, or in *continuous* manner by addition of dyes. Particle visualization has often been used for the determination of velocity fields in turbulent flows, with 2-D velocity fields determined by *particle-imaging-velocimetry (PIV)* [Adrian, 1986], or 2-D *particle-tracking-velocimetry (2-D PTV)* [Adamczyk & Rimai, 1988], and 3-D velocity fields and trajectories determined by *3-D PTV* [Papantoniou & Dracos, 1989], [Maas, 1991, 1992a].

In the experiments described in this paper, continuous visualization with dyes is used for the examination of a mixing process. A fluid (*fluid 2*) is injected into a vessel already filled with another fluid (*fluid 1*) and the two are mixed under turbulent flow conditions. Fluid 2 has been previously marked with fluo-

rescine which absorbs light of a certain wavelength and emits light of a different, usually higher, wavelength and can thus be made visible when illuminated by a laser beam of proper wavelength. When the fluids are being mixed, fluid 2 starts spreading and dissolving into fluid 1. The local concentration of fluid 2 inside a 3-D volume of the mixed fluids corresponds to the local fluorescine content. To visualize cross-sections of the mixed fluids we use a laser beam widened to a lightsheet by a cylindrical lens and aimed at the vessel (*LIF - laser induced fluorescence*). An image of the cross section of the mixed fluids thus illuminated by the laser sheet is captured by a high-speed solid state camera positioned above the vessel, with its optical axis perpendicular to the laser sheet. By moving the laser sheet in depth direction parallel to itself, and capturing digital images at fixed, differential time intervals, *3-D flow tomography datasets* are generated in a quasi-simultaneous manner (Fig. 1). By using a 256 x 256 pixel high-speed solid state camera with a maximum imaging rate of 500 frames per second, we generate volume datasets with a typical size of 256 x 256 x 50 voxels at a rate of 10 volume datasets per second.

These datasets are treated as 3-D images, with voxel gray values derived from the corresponding pixel gray values. By properly calibrating the imaging process, these voxel values are directly proportional to the fluorescein content of the corresponding finite 3-D element of the object space, and therefore they represent a local measure of fluid 2 content.

The aim of our experiments is to examine the mixing process in the vessel by determining the temporal development of the scalar concentration gradient field [Dahm et al, 1990] and the associated velocity fields.

## 2. HARDWARE CONFIGURATION

The experimental set-up for the acquisition of flow tomography data sequences was developed in a cooperation of the Laboratory for Technical Chemistry, the Institute of Hydromechanics and Water Resources Management and the Institute of Geodesy and Photogrammetry at ETH Zurich [Merkel et al., 1993] and it is shown in Fig. 1. The beam of a 26W Argon-ion laser is widened to a 2-D lightsheet by a cylindrical lens and is shifted step-wise in depth direction by a mirror mounted on a piezo element. A laser focus system assures minimum lightsheet thickness. This way the observation volume is scanned in depth direction and recorded by a high-speed camera synchronized with the stepper mirror. To avoid reflections, e.g. at bubbles in the water, an optical filter with a filter edge at  $\sim 525$  nm is used, which cuts off the wavelength of the laser (514 nm), so that only fluorescein emission ( $\sim 540$  nm) is being imaged.

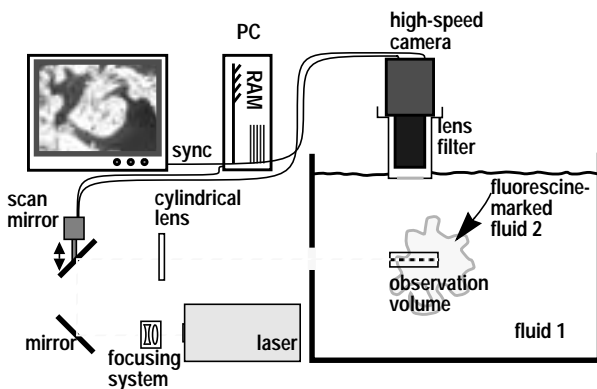


Fig. 1: Application Set-up

To allow for the recognition of the smallest scales of turbulence (*Kolmogorov scales*), a relatively small observation volume of  $15 \times 15 \times 3 \text{ mm}^3$  was chosen. The camera used in the system is an EG&G Reticon MC4256 [Maas, 1992b, 1993, 1994] and the resulting images are stored on a 64 MB sequence memory in RAM. For the observation volume of  $15 \times$

$15 \times 3 \text{ mm}^3$  a 3-D volume dataset of  $256 \times 256 \times 50$  voxels results in a voxel size of  $60 \times 60 \times 60 \mu\text{m}^3$  in object space. The minimum thickness of the scanning lightsheet attainable by the laser focusing system was also  $60 \mu\text{m}$ . The size of the sequence memory limits the duration of such an experiment to 1024 images ( $\sim 2$  seconds of data), which allows for the acquisition of 20 consecutive volume datasets of  $256 \times 256 \times 50$  voxels each.

Fig. 2 shows an example of a flow tomography sequence in a turbulent mixing process. The data consists of 5 volumina with 50 layers of  $256 \times 256$  pixels each in an observation volume of  $15 \times 15 \times 3 \text{ mm}^3$ ; the temporal resolution was 10 volumina per second.

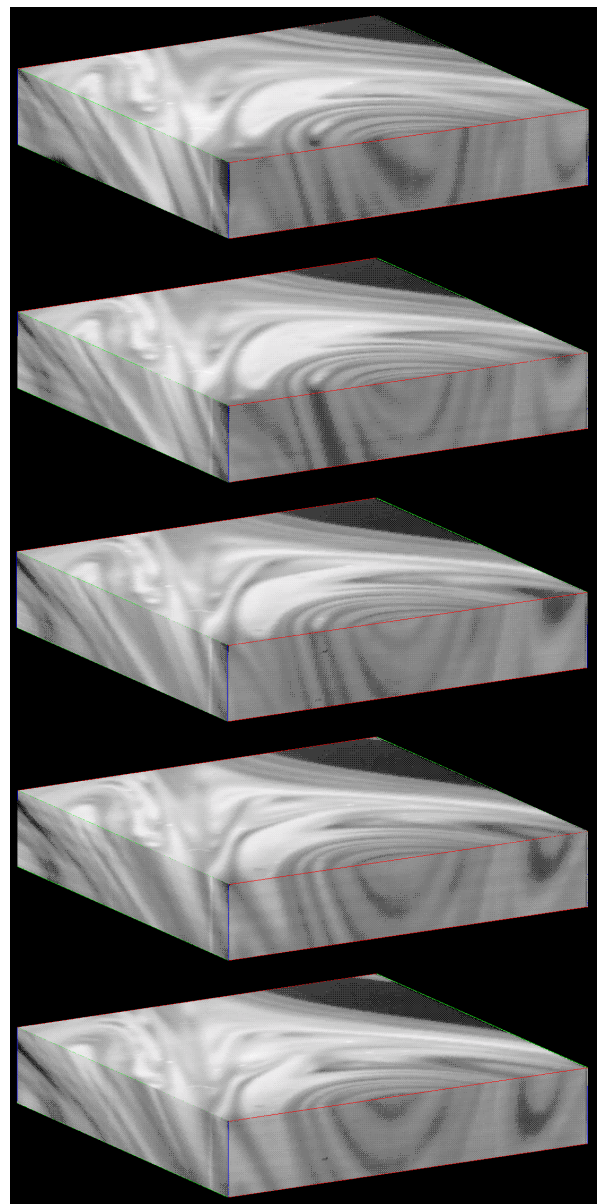


Fig. 2: Volume datasets: 5 consecutive volumina with 50 layers of 256 by 256 pixels each (total 16 MB = 0.5 seconds of flow data)

### 3. LEAST SQUARES MATCHING WITH VOXELS

*Least squares matching (LSM)* is a correlation technique, used in photogrammetry mainly for the establishment of correspondences [Grün, 1985], [Grün & Baltsavias 1988]. LSM was proven to be well suited for the establishment of temporal correspondences through structure tracking in 2-D image sequences [Papantoniou et al., 1990].

Least squares matching can be extended to a 3-D algorithm, working with 3-D volume data and voxels rather than 2-D images and pixels. To match two *cuboids*  $g_1(x, y, z)$ ,  $g_2(x, y, z)$  taken from two volume datasets  $V_1$  and  $V_2$ , cuboid  $g_1$  has to be transformed into  $g_2$  in a way that

$$g_1(x, y, z) = g_2(x, y, z) \quad (1)$$

To better accommodate noise and various radiometric and geometric dissimilarities in the imaging conditions of two 3-D datasets, which are not covered by eq. (3), a true error vector has to be added

$$g_1(x, y, z) - e(x, y, z) = g_2(x, y, z) \quad (2)$$

To express the geometric relationship between conjugate cuboids, the 6-parameter affine transformation used to relate conjugate patches in 2-D least squares matching has to be substituted by a 12-parameter 3-D affine transformation, as

$$\begin{aligned} x_2 &= a_0 + a_1x_1 + a_2y_1 + a_3z_1 \\ y_2 &= b_0 + b_1x_1 + b_2y_1 + b_3z_1 \\ z_2 &= c_0 + c_1x_1 + c_2y_1 + c_3z_1 \end{aligned} \quad (3)$$

with  $(a_0, b_0, c_0)$  being shifts,  $(a_1, b_2, c_3)$  scales, and  $(a_2, a_3, b_1, b_3, c_1, c_2)$  shears. Equation (2) can be linearized to yield observation equations as

$$\begin{aligned} g_1(x, y, z) - e(x, y, z) &= g_2^0(x, y, z) \\ &+ \frac{\partial g_2^0}{\partial x} dx + \frac{\partial g_2^0}{\partial y} dy + \frac{\partial g_2^0}{\partial z} dz \end{aligned} \quad (4)$$

With

$$x = \frac{\partial x}{\partial p_i} dp_i, \quad y = \frac{\partial y}{\partial p_i} dp_i, \quad z = \frac{\partial z}{\partial p_i} dp_i \quad (5)$$

$$i \in \{da_0, \dots, da_3, db_0, \dots, db_3, dc_0, \dots, dc_3\} \quad (6)$$

and by defining

$$\frac{\partial g_2^0}{\partial x} = g_x, \quad \frac{\partial g_2^0}{\partial y} = g_y, \quad \frac{\partial g_2^0}{\partial z} = g_z \quad (7)$$

the observation equations become

$$\begin{aligned} g_1(x, y, z) - e(x, y, z) &= g_2^0(x, y, z) + \\ &+ g_x da_0 + g_x x_2^0 da_1 + g_x y_2^0 da_2 + g_x z_2^0 da_3 \\ &+ g_y db_0 + g_y x_2^0 db_1 + g_y y_2^0 db_2 + g_y z_2^0 db_3 \\ &+ g_z dc_0 + g_z x_2^0 dc_1 + g_z y_2^0 dc_2 + g_z z_2^0 dc_3 \end{aligned} \quad (8)$$

and they can be grouped in a Gauss-Markov estimation model as

$$-e(x, y, z) = Ax - l; \quad P \quad (9)$$

$$E(e) = 0 \quad E(ee^T) = \sigma_0^2 P^{-1} \quad (10)$$

where the coefficient matrix  $A$ , observation vector  $l$  and vector of unknowns  $x$  are

$$\begin{aligned} A_i &= [g_x, g_x x_2^0, g_x y_2^0, g_x z_2^0, g_y, g_y x_2^0, g_y y_2^0, \\ &g_y z_2^0, g_z, g_z x_2^0, g_z y_2^0, g_z z_2^0]_i \end{aligned} \quad (11)$$

$$l = g_1(x, y, z) - g_2^0(x, y, z) \quad (12)$$

$$\begin{aligned} x^T &= [da_0, da_1, da_2, da_3, \\ &db_0, db_1, db_2, db_3, dc_0, dc_1, dc_2, dc_3] \end{aligned} \quad (13)$$

The values  $g_x, g_y, g_z$  are numeric gray value first derivatives, calculated either in  $g_1$  or in  $g_2$  or averaged over both. In contrast to typical photogrammetric applications a radiometric correction should be avoided this time, as it would interfere with the original radiometric calibration of the system.

The vector  $x$  of unknown parameters is determined by minimizing the sum of squares of the estimated residuals  $v(x, y, z)$  as

$$\hat{x} = (A^T P A)^{-1} (A^T P l) \quad ; \quad \hat{\sigma}_0^2 = \frac{v^T P v}{r} \quad (14)$$

The fact that  $g_2(x, y, z)$  actually contain stochastic quantities is neglected here (as typically done in LSM) to allow the use of the Gauss-Markov model [Grün & Baltsavias, 1988].

Velocity field components are deduced with subpixel accuracy from the adjusted shift parameters as

$$u = \left( \frac{a_0}{\Delta t}, \frac{b_0}{\Delta t}, \frac{c_0}{\Delta t} \right) \quad (15)$$

while information on the deformation behaviour of fluid elements is included in the remaining 9 transformation parameters  $(a_1, a_2, a_3, b_1, b_2, b_3, c_1, c_2, c_3)$ .

#### 4. ADDITIONAL CONSTRAINTS

Experience with 2-D matching has shown that there exist several gray value patterns for which some of the affine transformation parameters cannot be determined due to lack of sufficient contrast or high correlation between parameters [Grün & Stallmann, 1991]. Similar situations can occur in 3-D voxel matching. In such cases, either certain undeterminable parameters have to be excluded from the vector of unknowns, or additional constraints have to be introduced to strengthen the system. In the following some constraints for 3-D cuboid matching will be explained. It has to be mentioned that they arise from the special task of matching flow tomography sequences and are not necessarily valid for general applications of least squares image matching.

##### 4.1 Incompressibility Constraint

A fundamental property of the mixing fluids that are being used in the project described here is their incompressibility. That means that a cuboid, while changing its shape due to deformations, will have a constant volume. This fact can be exploited to prevent cuboids from uncontrolled growing or shrinking in the matching process.

The incompressibility constraint is formulated as

$$vol_1 = vol_2 \quad (16)$$

where  $vol_1$  is  $n_x \times n_y \times n_z$  and  $vol_2$  is calculated as the volume of the affine transformed  $vol_2$ . This yields an additional equation for the Gauss-Markov model

$$e_v = A_v x_v - l_v ; \quad v \quad (17)$$

$$A_v = [0, vol_x x_{2c}, vol_x y_{2c}, vol_x z_{2c}, 0, vol_y x_{2c}, vol_y y_{2c}, vol_y z_{2c}, 0, vol_z x_{2c}, vol_z y_{2c}, vol_z z_{2c}] \quad (18)$$

$$l_v = vol_1 - vol_2 \quad (19)$$

The derivatives  $\partial vol / \partial p$  are calculated numerically.

##### 4.2 Intensity Constraint

This is a highly specialized constraint, stemming from the particular nature of the application at hand, forcing the gray value sums  $sg$  within cuboids  $g_1$ ,  $g_2$  to be equal. This constraint can only be valid in 3-D, since for 2-D applications fluorescence might simply move into the third dimension and violate this criterion. In 3-D it is only valid when linearity between fluorescence content and voxel gray values can be assumed. The basic formulation of the condition

$$sg_1 = sg_2 \quad (20)$$

yields an additional equation for the Gauss-Markov

model

$$-e_t = A_t x - l_t ; \quad P_t \quad (21)$$

$$A_t = [sg_x, sg_x x_{2c}, sg_x y_{2c}, sg_x z_{2c}, sg_y, sg_y x_{2c}, sg_y y_{2c}, sg_y z_{2c}, sg_z, sg_z x_{2c}, sg_z y_{2c}, sg_z z_{2c}] \quad (22)$$

$$l_t = sg_1 - sg_2 \quad (23)$$

where  $sg_x$ ,  $sg_y$ ,  $sg_z$  are the numeric first derivatives of gray value sum and  $(x_{2c}, y_{2c}, z_{2c})$  is the transformed central voxel of the  $g_2$  cuboid. Note that  $sg_2$  is the total intensity over the volume covered by the transformed cuboid  $g_2$ , not over the matrix  $g_2$ .

This constraint may be very valuable especially for preventing drifts of the scale parameters of the affine transformation in regions of low contrast, but it may be extremely dangerous in general applications. If for example a bright signalized target on dark background is imaged with different scales by two cameras in a close range photogrammetric application and one tries to match from a larger patch in  $g_1$  to a smaller patch in  $g_2$ , the basic condition of continuity of total intensity is hurt implicitly, and cannot even be fulfilled by changed scale parameters, as no intensity can be gained. In this case the numeric derivatives  $sg_x$ ,  $sg_y$ ,  $sg_z$  in  $g_1$  remain constant and convergence is not achieved.

##### 4.3 Smoothness of Velocity Field

This constraint is based on the assumption that the sampling frequency is sufficiently high, ensuring that consecutive datasets are correlated to a certain extent and Lagrangian acceleration is relatively low. For its implementation matching is no longer performed with only two datasets at time instances  $T_i \rightarrow T_{i+1}$ , but at least a third dataset  $T_{i+2}$  is also available and correlation between the parameters of the affine transformations  $T_i \rightarrow T_{i+1}$  and  $T_{i+1} \rightarrow T_{i+2}$  is assumed. The constraint can be formulated as additional observation equations for the parameters. Considering for example the shift parameter in x-direction, the associated equation becomes

$$a_{0_{(0 \rightarrow 2)}} = 2 \cdot a_{0_{(0 \rightarrow 1)}} \Rightarrow -v = 2 \cdot a_{0_{(0 \rightarrow 1)}} - a_{0_{(0 \rightarrow 2)}} \quad (24)$$

The remaining 11 equations can be formulated accordingly. The smoothness constraints produce additional equations

$$e_s = A_s x - l_s ; \quad P_s \quad (25)$$

where

$$A_s = [2I_{12} \quad -I_{12}] \quad (26)$$

with  $I_{12}$  being the  $12 \times 12$  unit matrix, and

$$I_s = \begin{bmatrix} a_{0(0 \rightarrow 2)} - 2 \cdot a_{0(0 \rightarrow 1)} \\ a_{1_{0 \rightarrow 2}} - 1 - 2 \cdot (a_{1_{0 \rightarrow 1}} - 1) \\ a_{2_{(0 \rightarrow 2)}} - 2 \cdot a_{2_{(0 \rightarrow 1)}} \\ a_{3_{(0 \rightarrow 2)}} - 2 \cdot a_{3_{(0 \rightarrow 1)}} \\ b_{0(0 \rightarrow 2)} - 2 \cdot b_{0(0 \rightarrow 1)} \\ b_{1_{(0 \rightarrow 2)}} - 2 \cdot b_{1_{(0 \rightarrow 1)}} \\ b_{2_{0 \rightarrow 2}} - 1 - 2 \cdot (b_{2_{0 \rightarrow 1}} - 1) \\ b_{3_{(0 \rightarrow 2)}} - 2 \cdot b_{3_{(0 \rightarrow 1)}} \\ c_{0(0 \rightarrow 2)} - 2 \cdot c_{0(0 \rightarrow 1)} \\ c_{1_{(0 \rightarrow 2)}} - 2 \cdot c_{1_{(0 \rightarrow 1)}} \\ c_{2_{(0 \rightarrow 2)}} - 2 \cdot c_{2_{(0 \rightarrow 1)}} \\ c_{3_{0 \rightarrow 2}} - 1 - 2 \cdot (c_{3_{0 \rightarrow 1}} - 1) \end{bmatrix} \quad (27)$$

By manipulating the associated weight matrix  $P_s$  the constraint can be invalidated ( $P_s = 0$ ), or strictly enforced ( $P_s \rightarrow \infty$ ) in which the parameter sets of consecutive transformations are forced to be identical. Eq. 19 shows the implementation for three datasets  $T_i \rightarrow T_{i+1} \rightarrow T_{i+2}$ . It can be straightforwardly extended to more consecutive time steps  $T_i \rightarrow T_{i+1} \rightarrow \dots \rightarrow T_{i+n}$ .

#### 4.4 Multi-Patch Matching

This geometric constraint forces neighbouring cuboids to remain fit together after their boundaries are reshaped by the matching adjustment. An analogous approach has been formulated for DTM generation applications by [Grün, 1985] and [Rosenholm, 1986]. For the 3-D implementation [Maas, 1994] it is realized by adding observation equations for the coincidence of the corner pixels of neighboring elements (7 neighbors at 8 corner voxels).

This multi-patch constraint implies that parameters of single cuboids cannot be solved independently anymore. In the extreme case, the transformation parameters of all cuboids of the complete dataset have to be estimated together in one system. Combined with the smoothness constraint which ties multiple datasets together, the resulting equation system can become extremely large. Despite its sparsity, it will impose immense computational burdens. In a realistic experiment with 256x256x64 voxels per each dataset and a cuboid size of e.g. 17x17x17 voxels with smoothness constraints applied only for consecutive datasets, a total of 24576 unknowns per volume dataset would have to be solved. It is clear that such a system would be computationally too expensive and therefore the equation system has to be split into smaller, manageable parts. A promising idea is to search for

cuboids with sufficient contrast for a independent solution in a first step and then triangulate the volume dataset with a tetrahedra-structure, within which the multi-patch constraint and the smoothness criterium will have to be applied.

## 5. GLOBAL SOLUTION

A global matching solution is obtained for a single pair of cuboids by the introduction of the *incompressibility* and *intensity* constraints as

$$\hat{x} = (A^T P A + A_V^T P_V A_V + A_t^T P_t A_t)^{-1} (A^T P I + A_V^T P_V I_V + A_t^T P_t I_t) \quad (28)$$

Considering more than two consecutive cuboids, a *multitemporal* global matching solution is obtained by further introducing the *smoothness of velocity field* constraint as

$$\hat{x} = (A^T P A + A_V^T P_V A_V + A_t^T P_t A_t + A_s^T P_s A_s)^{-1} (A^T P I + A_V^T P_V I_V + A_t^T P_t I_t + A_s^T P_s I_s) \quad (29)$$

In the above equation, all matrices contain information from all involved templates, and matrices in equation (28) are submatrices of their counterparts in equation (29). The introduction of a *multi-patch* constraint would allow us to tie multiple patches in a multitemporal matching adjustment.

## 6. STRATEGIES

Considering the large amount of data associated with 3-D image sequences in general, and the multi-directional velocities involved in this specific application, it is evident that the devison of an efficient matching strategy can optimize the application of the excellent matching tool which is the above described 3-D least squares matching. In particular, the task of initial value selection for the matching parameters (especially for the three shifts  $a_o$ ,  $b_o$  and  $c_o$ ) is crucial since erroneous selection can cause matching to fail. The use of a hierarchical strategy can greatly facilitate this task.

Multigrid hierarchical strategies proceed in a number of levels, from coarse to fine, by employing successively refined grid structures [Li, 1989]. Applied to the matching problem at hand, the implementation of a *3-D multigrid hierarchical strategy* proceeds by selecting

- a 3-D grid structure, defined by its grid element size  $(r_x, r_y, r_z)$ , to cover a 3-D dataset, and
- a corresponding cuboid size  $(c_x, c_y, c_z)$ .

For this initial configuration (*level 1*) matching is performed using cuboids of the chosen size

centered at the grid positions. Depending on the cuboid and grid element sizes, neighboring cuboids can share common borders ( $c_i = c_j$  where  $i \in \{x, y, z\}$ ), overlap ( $c_i < c_j$ ), or not overlap at all ( $c_i > c_j$ ). Obviously, the multi-patch constraint can only be applied in the first case, while overlapping cuboids will produce velocity data correlated to a certain extent. For sufficiently large cuboid sizes trivial initial approximations can be provided and a matching solution can still be achieved. The matching solution  $\hat{x}^1$  from this first configuration provides the necessary information to update the conjugate positions. Using these results we proceed on the next level, at which the grid element and/or cuboid sizes become smaller. At this level, approximations for the new adjustment solution are based on the matching solution  $\hat{x}^1$  of the previous level. These approximations need not be restricted solely to the obvious choice of the three shifts, but could include the scale and shear parameters as well. However, to alleviate computational burdens, it is advisable in low, coarse levels to solve only for the shift parameters which are typically more crucial for successful matching. The procedure continues with approximations for *level*  $i+1$  provided directly or indirectly (via interpolation) from the matching adjustment solutions of *level*  $i$ . Thus is devised a *globally iterative process* for which different levels correspond to a change in the number and/or size of the cuboids, and minor iterations (local adjustment solutions) form single iterative steps of the complex multigrid solution procedure. Matching results from coarse grid levels correspond to low frequency components of the velocity vectors, while in finer levels the effect of high frequency velocity components is also considered.

To optimize the potential of this solution process, a *modified 3-D multigrid hierarchical strategy* can be used. Once a grid structure has been defined, grid locations can be modified by the employment of an interest operator, to coincide with distinct voxels in the vicinity of their original positions. The application of Förstner's operator [Förstner, 1986] to 2-D image windows allows the detection of distinct interest points as points with circular and small confidence ellipses. The extension of this operator for application to 3-D datasets proceeds by analyzing for each point the size and sphericity of the local confidence ellipsoid. The associated normal matrix  $N$  is

$$N = \begin{bmatrix} \Sigma g_x^2 & \Sigma g_x g_y & \Sigma g_x g_z \\ \Sigma g_x g_y & \Sigma g_y^2 & \Sigma g_y g_z \\ \Sigma g_x g_z & \Sigma g_y g_z & \Sigma g_z^2 \end{bmatrix} \quad (30)$$

and contains information on whether local gray value

variations make a voxel distinct or not. The trace of  $N$  and its eigenvalues (or their product in the determinant) uniquely define the distinctness of the associated voxel. The roundness criterion

$$Q = \frac{4 \det N}{\text{tr}^2 N} \quad (31)$$

and the precision criterion

$$W = \frac{2 \det N}{\text{tr} N} \quad (32)$$

can be calculated in direct analogy to their 2-D counterparts [Förstner, 1993]. When the value of either criterion is very small, at least one of the three associated eigenvalues is approaching 0, denoting the presence of a nearly linear edge pattern. On the other hand, points for which both  $Q$  and  $W$  are above acceptable limits are considered 3-D interest points. It is worth mentioning that the  $2 \times 2$   $N_{ij}$  submatrices formed along the diagonal of matrix  $N$

$$N_{ij} = \begin{bmatrix} \Sigma g_i^2 & \Sigma g_i g_j \\ \Sigma g_i g_j & \Sigma g_j^2 \end{bmatrix}; \quad i \neq j \text{ and } i, j \in \{x, y, z\} \quad (33)$$

are the normal matrices in the  $(x,y)$ ,  $(y,z)$  and  $(x,z)$  planes. Their roundness and precision indices,  $q_{ij}$  and  $w_{ij}$  respectively, express independently in each of these planes the potential presence of interest points. The product of these indices can provide an approximation to the  $Q$  and  $W$  criteria of equations 31 and 32.

Interest point search is performed within a rather small 3-D area centered on the initial grid location. The size of the search area is defined by the grid element and cuboid sizes, to avoid redundant operations and extreme computational burdens. In the case where the search area coincides with the cuboid size, the elements of the  $N_{ij}$  matrix of Eq. 32 will also be elements of the  ${}^T P A$  matrix of Eq. 14 and some repetition can thus be avoided.

3-D interest points detected by this procedure will offer excellent matching potential. If an interest point cannot be found within the search area, the original grid point can be used, but information from the above interest analysis can be used to remove certain undeterminable parameters from the matching solution which will follow.

The advantage associated with the use of distinct cuboids for matching is twofold:

- From the *photogrammetric point of view*, cuboids centered at such positions provide sufficient contrast and good determinability, ensuring robust matching solutions and reliable results.

- From the specific *application point of view*, interest points correspond to characteristic locations within edges, and therefore they better describe the interaction of the two fluids and the mixing process itself.

## 7. SOME RESULTS

The 3-D implementation of least squares matching shown in this paper has been programmed and combined with the constraints shown in chapters 4.1 - 4.3. The multi-patch constraint discussed in chapter 4.4 does still need some work in order to keep the computational effort on a reasonable level. First tests have shown that due to the contrast situation in the flow tomography sequence shown in Fig. 2 the cuboids for least squares matching had to be chosen relatively large (typically about 15x15x15 voxels) and the introduction of the constraints was often necessary. Fig. 3 shows shifts and deformations of a typical cuboid through the iterations.

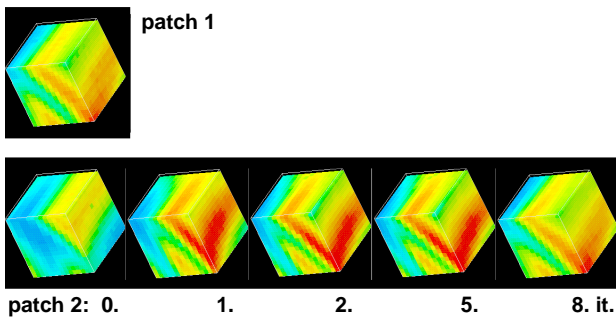


Fig. 3: 15 x 15 x 15 voxel cuboid through 8 iterations

In some regions of the datasets no velocity vectors could be determined, in other regions only certain parameters of the 3-D affine transformation could be determined. The decision, whether a vector could be determined at all and which transformation parameters could be determined, was met after a contrast check in the cuboid and reliability tests.

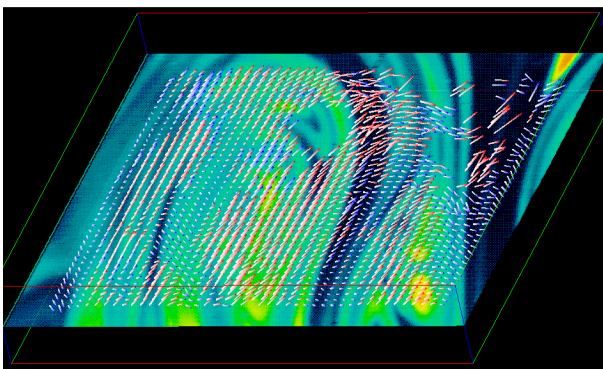


Fig. 4: Result - velocity vectors centered at a data layer

A partial result displaying velocity vectors computed for the center layer of one of the datasets of Fig. 2 is

shown in Fig. 5. Only the incompressibility constraint was used, the other constraints were disabled. The least squares matching yielded a  $\sigma_0$  of 2-5 greyvalues for most of the cuboids, the standard deviations of the shift parameters were  $\sim 1/30 - 1/50$  of a voxel, which corresponds to  $\sim 1-2\mu\text{m}$  in object space. A total of 1675 velocity vectors could be computed.

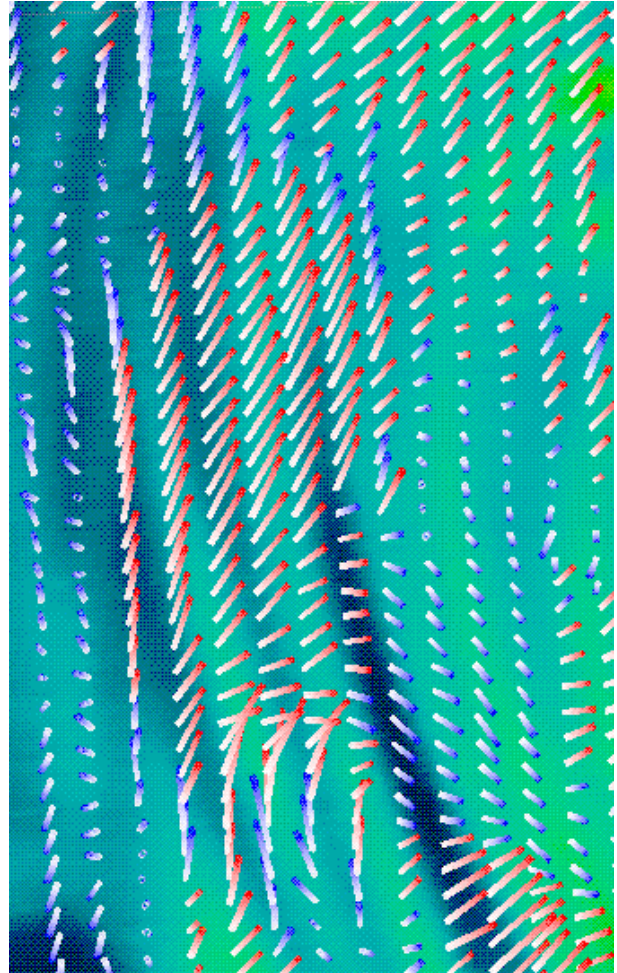


Fig. 5: Zoom on Fig. 5

Fig. 5 shows a zoom on this dataset showing a high local correlation in the velocity field, which was over-sampled, but computed without the multi-patch constraint.

## REFERENCES

1. Adamczyk A. & L. Rimai (1988): *2-Dimensional Particle Tracking Velocimetry (PTV): Technique and Image Processing Algorithms*, Experiments in Fluids, Vol. 6, pp. 373-380.
2. Adrian R. (1986): *Multi-Point Optical Measurements of Simultaneous Vectors in Insteady Flow - A Review*, The International Journal of Heat and Fluid Flow, Vol. 7, No. 2, pp. 127 - 145.
3. Dahm J.A., K.B. Southerland & K.A. Buch (1990): *Four-Dimensional Laser Induced Fluorescence Measurements of Conserved Scalar*

- Mixing in Turbulent Flows*, 5th Int. Symposium on the Application of Laser Techniques to Fluid Mechanics, Lisbon, 9.-12.7.1990.
4. Förstner W. (1986): *A Feature Based Correspondence Algorithm for Image Matching*, IAPRS, Vol. 26, Part 3/3, pp. 150-166.
  5. Förstner W. (1993): *Image Matching*, in Computer and Robot Vision Vol. II (Haralick R.M. & Shapiro L.G.), Addison-Wesley, Reading, MA, pp. 289-378.
  6. Grün A. (1985): *Adaptive kleinste Quadrate Korrelation und geometrische Zusatzinformationen*, Vermessung, Photogrammetrie und Kulturtechnik 9/85, pp. 309-311.
  7. Grün A. & E. Baltsavias (1988): *Geometrically Constrained Multiphoto Matching*, Photogrammetric Engineering, Vol. 54, No. 5, pp. 633 - 641.
  8. Grün A. & D. Stallmann (1991): *High-accuracy edge-matching with an extension of the MPGC matching algorithm*, Proceedings Industrial Vision Metrology, SPIE Volume 1526, pp.42-55.
  9. Li. M. (1989): *Hierarchical Multi-Point Matching with Simultaneous Detection and Location of Breaklines*, Ph.D. Thesis, Department of Photogrammetry, The Royal Institute of Technology, Stockholm.
  10. Maas H.-G. (1991): *Digital Photogrammetry for Determination of Tracer Particle Coordinates in Turbulent Flow Research*, Photogrammetric Engineering & Remote Sensing Vol. 57, No. 12, pp. 1593-1597.
  11. Maas H.-G. (1992a): *Digitale Photogrammetrie in der dreidimensionalen Strömungsmeßtechnik*, Dissertation Nr. 9665, ETH Zürich.
  12. Maas H.-G. (1992b): *High-Speed Solid State Camera Systems for Digital Photogrammetry*, IAPRS, Vol. 29, Part B5, pp. 709-713.
  13. Maas H.-G. (1993): *Techniques for Destriping of Digital Images*, ISPRS Com. I Workshop on Digital Sensors and Systems, Trento, 21-25. 6. 1993.
  14. Maas H.-G. (1994): *A Highspeed Camera System for the Acquisition of Flow Tomography Sequences for 3-D Least Squares Matching*, IAPRS, Vol. 30, Part 5, pp. 241-249.
  15. Merkel G., T. Dracos, P. Rys & F. Rys (1993): *Flow Tomography by Laser Induced Fluorescence*, XXV IAHR Congress, Tokyo, 30. 8. - 3. 9. 1993.
  16. Papantoniou D. & T. Dracos (1989): *Analyzing 3-D Turbulent Motions in Open Channel Flow by Use of Stereoscopy and Particle Tracking*, in: Advances in Turbulence 2 (H.-H. Hernholz & H.E. Fiedler eds.), Springer Verlag, Heidelberg.
  17. Papantoniou D., H. Bühler & T. Dracos (1990): *On the Internal Structure of Thermals and Momentum Puffs*, International Conference on Physical Modelling of Transport and Dispersion, MIT, 7.-10. August.
  18. Rosenholm D. (1986): *Accuracy Improvement of Digital Matching for Evaluation of Digital Terrain Models*, IAPRS, Vol. 26, Part 3/2, pp. 573-587.